Localized patterns, stationary fronts, and snaking in bistable ranges of spots and stripes

Hannes Uecker, Daniel Wetzel
Institut für Mathematik, Universität Oldenburg, D26111 Oldenburg
hannes.uecker@uni-oldenburg.de daniel.wetzel@uni-oldenburg.de

April 8, 2013

arXiv:1304.1723v1 [math.DS] 5 Apr 2013

Abstract

For a stationary reaction-diffusion system on a two dimensional domain we use the continuation and bifurcation software `pde2path` to numerically calculate branches of fronts between different patterns, and localized solution branches, for instance spots embedded in stripes and vice versa. Some of these branches show a snaking behaviour in parameter space. We use the Ginzburg-Landau reduction to approximate the locations of these branches by a Maxwell point for the associated Ginzburg–Landau system.

Keywords: Turing patterns, pinning, snaking, Ginzburg–Landau approximation, Maxwell point
MSC: 35J60, 35B32, 35B36, 65N30

1 Introduction

Homoclinic snaking refers to the back and forth oscillation in parameter space of a branch of stationary localized patterns for some pattern forming partial differential equation (PDE). Two standard models are the quadratic–cubic Swift–Hohenberg equation (SHe)

$$\partial_t u = -(1+\Delta^2)^2 + \lambda u + \nu u^2 - u^3, \quad u = u(t,x) \in \mathbb{R}, \quad x \in \Omega \subset \mathbb{R}^d, \tag{1}$$

and the cubic–quintic SHe

$$\partial_t u = -(1+\Delta^2)^2 + \lambda u + \nu u^3 - u^5, \quad u = u(t,x) \in \mathbb{R}, \quad x \in \Omega \subset \mathbb{R}^d, \tag{2}$$

with suitable boundary conditions if $\Omega \neq \mathbb{R}^d$, and where $\lambda \in \mathbb{R}$ is the linear instability parameter and $\nu > 0$. In both equations the trivial solution $u \equiv 0$ is stable for $\lambda < \lambda_c := 0$, where in the 1D case $d = 1$ we have a pitchfork bifurcation of periodic solutions with period near 2π. For $\nu > \nu_0 \geq 0$, with $\nu_0 = \sqrt{27/38}$ for (1) and $\nu_0 = 0$ for (2), the bifurcation is subcritical and the periodic branch starts with unstable small solutions u_- and turns around in a fold at $\lambda = \lambda_0(\nu) < 0$ to yield $\mathcal{O}(1)$ amplitude stable periodic solutions. Thus, for $\lambda_0 < \lambda < \lambda_c$ there is a bistable regime of the trivial solution and $\mathcal{O}(1)$ amplitude rolls.

In the simplest case the localized patterns then consist of 1D rolls over a homogeneous background $u = 0$, and in each pair of turns in the snake the localized pattern grows by adding a pair of rolls on both sides, and this continues for ever over the infinite line. See, e.g., [BK06, BK07, BKL$^+$09] for seminal results in this setting, and [CK09, DMCK11] for detailed analysis using a Ginzburg–Landau formalism and beyond all order asymptotics. 1D snaking in finite domains has been studied in, e.g., [HK09, Daw09]. In 2D, by rotational invariance, depending on the domain

and boundary conditions multiple patterns may bifurcate from $u \equiv 0$ at $\lambda = 0$, for instance so called straight rolls, and hexagonal and rectangular spots. There are a number of studies of localized patterns over two dimensional domains [LSAC08, ALB$^+$10], often combining analysis and numerics, and in more complicated systems like fluid convection [LJBK11], but all these essentially consider patterns embedded in a homogeneous background. Already in [Pom86] it is pointed out that "pinned" fronts connecting stripes and hexagonal spots may exist in reaction-diffusion systems as a codimension 0 phenomenon in parameter space, i.e., for a whole interval of parameters, and similar ideas were also put forward non–rigorously in [MNT90] with the 2D quadratic–cubic SHe (2) as an example, see in particular [MNT90, Appendix C]. Such a pinned front is observed in [HMBD95] for (2) by time integration, but so far no studies of branches of stationary solutions involving different 2D patterns seem available.

Here we consider a standard model problem for predator (u) prey (v) reaction diffusion systems, namely

$$\partial_t U = D\Delta U + N(U,\lambda), \qquad N(U,\lambda) = \begin{pmatrix} -u + u^2 v \\ \lambda - u^2 v \end{pmatrix}, \tag{3}$$

with $U = (u,v)(t,x,y) \in \mathbb{R}^2$, diffusion matrix $D = \left(\begin{smallmatrix} 1 & 0 \\ 0 & d \end{smallmatrix}\right)$, d fixed to $d = 60$, and bifurcation parameter $\lambda \in \mathbb{R}_+$. The reaction term N of (3) is a special version of the Schnakenberg [Sch79] and Selkov model [Sel68]. In particular we consider the stationary system

$$D\Delta U + N(U,\lambda) = 0. \tag{4}$$

The unique spatially homogeneous solution of (4) is $w^* = (\lambda, 1/\lambda)$. We write (4) in the form

$$\partial_t w = L(\Delta)w + G(w), \tag{5}$$

with $w = U - w^*$ and $L(\Delta,\lambda) = J(\lambda) + D\Delta$, where J is the Jacobian of N in w^*. For $\mathbf{k} = (m,n) \in \mathbb{R}^2$ we have $L(\Delta,\lambda)e^{i(mx+ny)} = \hat{L}(\mathbf{k},\lambda)e^{i(mx+ny)}$, where $\hat{L}(\mathbf{k},\lambda) = J(\lambda) - Dk^2$, $k := \sqrt{m^2+n^2}$, and thus we also write $\hat{L}(k,\lambda)$. The eigenvalues of $\hat{L}$ are given by $\mu_\pm(\mathbf{k},\lambda) = \mu_\pm(k,\lambda) = \frac{\mathrm{tr}\hat{L}(k,\lambda)}{2} \pm \sqrt{\left(\frac{\mathrm{tr}\hat{L}(k,\lambda)}{2}\right)^2 - \det\hat{L}(k,\lambda)}$. Following [Mur89, Chapter 14] we find that in $\lambda_c = \sqrt{d}\sqrt{3-\sqrt{8}} \approx 3.2085$ we have $\mu_+(\mathbf{k},\lambda_c) = 0$ for all vectors $\mathbf{k} \in \mathbb{R}^2$ of length $k_c = \sqrt{\sqrt{2}-1} \approx 0.6436$, and all other $\mu_\pm(\mathbf{k},\lambda_c) < 0$, i.e., there is a Turing bifurcation at λ_c, with critical wave vectors $\mathbf{k} \in \mathbb{R}^2$ in the circle $|\mathbf{k}| = k_c$. The most prominent Turing patterns near bifurcation are stripes and (hexagonal) spots and can be expanded as

$$\begin{aligned} U &= w^* + 2\left(A\cos(k_c x) + B\cos\left(\frac{k_c}{2}\left(-x+\sqrt{3}y\right)\right) + B\cos\left(\frac{k_c}{2}\left(-x-\sqrt{3}y\right)\right)\right)\Phi + \text{h.o.t.} \\ &= w^* + 2\left(A\cos(k_c x) + 2B\cos\left(\frac{k_c}{2}x\right)\cos\left(\frac{k_c}{2}\sqrt{3}y\right)\right)\Phi + \text{h.o.t.}, \end{aligned} \tag{6}$$

where $\Phi \in \mathbb{R}^2$ is the critical eigenvector of $\hat{L}(k_c,\lambda_c)$, and h.o.t. stands for higher order terms. The amplitudes $2A, 2B \in \mathbb{R}$ (where the factor 2 has been introduced for consistency with §3) of the corresponding Turing pattern depend on λ, with $A = B = 0$ at bifurcation.

In §2 we numerically calculate Turing patterns for (4), including so called so called mixed modes, and, moreover, find some branches of stationary solutions which involve different patterns, namely

(a) fronts between stripes and spots, and associated localized patterns, e.g., stripes localized in one direction on a background of hexagons, and vice versa;

(b) fully 2D localized patches of hexagons over a homogeneous background.

The patterns in (a) come in two regimes: one "hot" which is rather far from the primary bifurcation at λ_c; one "cold", with λ closer to λ_c. Of these, only the "hot" branches show snaking behaviour in our numerical simulations, and we conjecture that the non–snaking of the "cold" branches (and also of the fully localized branches (b)) is due to the fact that subcriticality of the primary bifurcation is rather weak. In §3 we relate our numerical results to arguments derived from the Ginzburg-Landau reduction. The main result is the calculation of three Ginzburg–Landau Maxwell points which give predictions for the λ–ranges of the fronts and localized patterns in the full system (4). In §4 we close with a brief discussion.

The results are not specific to the model system (4) but can be expected in any reaction diffusion system (over sufficiently large domains) with a bistability between different patterns which allow homo–or heteroclinic connections in the associated Ginzburg–Landau system.

2 Numerical Results

2.1 Stripes, spots, and beans

We use the bifurcation and continuation software `pde2path` [UWR12] to numerically calculate patterns for (4), and their stability, over the domain $\Omega = [-l_x, l_x] \times [-l_y, l_y]$, $l_x = 2l_1\pi/k_c$, $l_y = 2\delta l_2\pi/(\sqrt{3}k_c)$, with Neumann boundary conditions, which was chosen to accomodate the basic stripe and spot patterns. Here $l_1, l_2 \in \mathbb{N}$, and the slight "detuning" $\delta \approx 1$ is used to unfold the multiple bifurcation at $\lambda = \lambda_c$ since `pde2path` currently only deals with simple bifurcations.

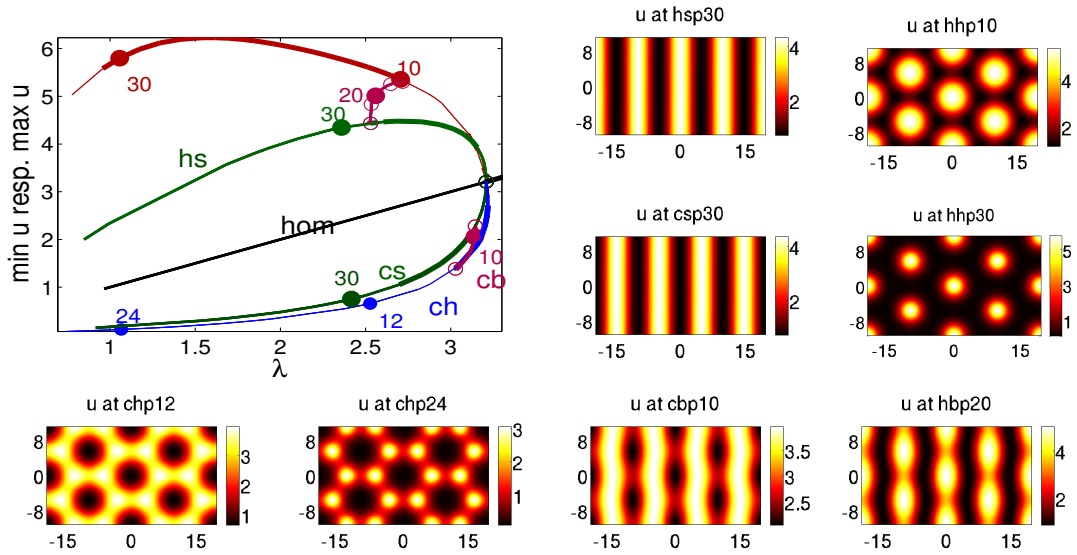

Figure 1: Bifurcation diagram and example solutions of (4) obtained with `pde2path` over the "2×2"–domain $\Omega = [-l_x, l_x]\times[-l_y, l_y]$ with Neumann boundary conditions, l_x=$4\pi/k_c$, l_y=$4\pi/(\sqrt{3}k_c)$, $k_c = \sqrt{\sqrt{2}-1}\approx 0.6436$. The branch `hom` are the homogeneous solutions, `hs` the hot (up) stripes, `cs` the cold (down) stripes, `hh` the hot spots, and `ch` the cold spots. For instance `hsp30` stands for the 30^{th} point of `hs`. `hb` and `cb` are mixed modes, which we call hot and cold beans, respectively. For `hs`, `hh`, and `hb` we plot the maximum of u, and the minimum for `cs`, `ch`, and `cb`. Stable and unstable parts of branches are represented by thick and thin lines, respectively. In particular, except for `hhp10, hhp30` all displayed patterns are unstable. Only a small selection of bifurcation points is indicated by ∘.

In Fig. 1 we use $\delta = 0.99$ and $l_1 = l_2 = 2$, which we call a 2×2 domain as in both directions 2 spots "fit". The main panel shows a part of the very rich bifurcation diagram (BD). Following biological terminology we classify the stripes ($A \neq 0$, $B = 0$) into hot (also called "up") stripes (`hs`, $A > 0$) and cold (also called "down") stripes (`cs`, $A < 0$), which exhibit a maximum respectively a minimum at $x = 0$. They are $2\pi/k_c$-periodic in the horizontal direction, bifurcate in a supercritical pitchfork, and are stable from $\lambda_{sb} \approx 3.15$ to $\lambda_{se} \approx 2.51$, where here and henceforth the first index of the bifurcation parameter λ stands for the branch and second for **e**nding or **b**eginning of stability. The (hexagonal) spots ($A = B \neq 0$) can be classified into hot spots (`hs`, $A = B > 0$) and cold spots (`cs`, $A = B < 0$), which have a maximum resp. a minimum in the center of every spot. They are $4\pi/k_c$-periodic in the horizontal and $4\pi/(\sqrt{3}k_c)$-periodic in the vertical direction. The spot branch bifurcates transcritically from the homogeneous branch at $\lambda = \lambda_c$, i.e., it starts in a saddle node or fold bifurcation $\lambda_{cb} \approx 3.22$, and the stability region of the cold spots begins at the fold and ends in $\lambda_{ce} \approx 3.03$. The hot spots are stable from $\lambda_{hb} \approx 2.73$ to $\lambda_{he} \approx 0.98$.

Thus, there is a bistable range of cold stripes and cold spots for $\lambda \in (\lambda_{ce}, \lambda_{sb})$, of hot stripes and hot spots for $\lambda \in (\lambda_{se}, \lambda_{hb})$, and of cold spots and the homogeneous solution for $\lambda \in (\lambda_c, \lambda_{cb})$. A branch of "skewed hexagon" or "mixed mode" solutions of the form (6) with $A < B < 0$ bifurcates subcritically from the cold spot branch `ch` in λ_{ce} and terminates on the cold stripe branch `cs` in λ_{sb}. We call this type of solutions cold *beans* (`cb`), cf. [Yan04]. There is also a branch `hb` of hot beans with $A > B > 0$ which bifurcates subcritically from the hot stripe branch `hs` in λ_{se} and terminates on the hot spot branch `hh` in λ_{hb}. We always plot the patterns of u. If we have a hot pattern for u, then v is a cold pattern and vice versa. This follows from the predator-prey structure of the reaction term N of (4).

Remark 2.1. For all these patterns the discrete symmetry $\mathcal{S} = S_{2\pi/k_c}$ given by the shift by $2\pi/k_c$ in the horizontal direction yields a solution as well. The stripes are of course invariant under $\mathcal{S}$, but for the hexagonal spots the shifts generate new branches $\mathcal{S}$`hh` and $\mathcal{S}$`ch`. These make the plotting of the BD a bit complicated graphically. Therefore, in Fig. 2 we repeat the BD from Fig. 1 in a schematic way, with ordinate $u(0,0)$, i.e., u in the center of the domain, and add the branches of shifted hexagons. The bean branches `hb` and `cb` then both take part in a "loop" involving shifted beans and so called rectangles which again can be expanded as in (6) but with $|A| \leq |B|$. This can be worked out on the level of amplitude equations, see §3, and it is also recovered by our numerics for the full system. The behaviour described below like snaking branches bifurcating from hot beans obviously transfers to branches related by $\mathcal{S}$, while on the rectangle branches some different behaviour occurs, which here we do not study, but see [WF13]. In the following we mainly focus on the `hb` and `cb` branches, and also mostly restrict to following just one direction at bifurcation. ⌋

Remark 2.2. The main regime of interest to us is $\lambda \in [2.5, 3.22]$, and below $\lambda \approx 2.5$ all branches plotted except `hh` are unstable. We plotted a somewhat larger bifurcation picture since, e.g., on the `ch` branch some interesting patterns occur. ⌋

Remark 2.3. `pde2path` uses the Matlab FEM `pdetoolbox` to discretize elliptic PDEs like (4), including some error estimators and adaptive mesh–refinement, see [UWR12] for details. In Fig. 1 we used a regular "base mesh" of 20.000 triangles which, e.g., on the beans branch is refined to about 60.000 triangles on average. Moreover, for all solutions calculated the mesh can be further refined to yield arbitrary small error estimates without visible changes to the solutions. Calculation time for the full BD in Fig. 1 on a quad core desktop PC is about 40 Minutes.

The rather large numbers of triangles was needed mainly in order to avoid uncontrolled branch switching, and it is the large number of different branches which makes the continuation and bifurcation numerics of (4) demanding. For instance, on the 2×2 domain the first 10 bifurcations from the homogeneous branch occur between $\lambda = \lambda_c \approx 3.2085$ and $\lambda_{10} = 3.1651$. On larger

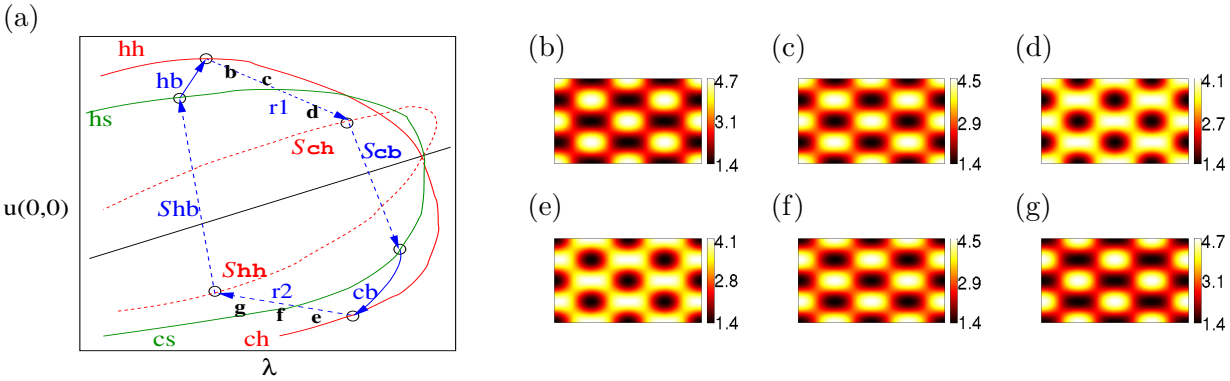

Figure 2: (a) Schematic BD with $u(0,0)$ as ordinate. Additional branches compared to Fig. 1 are dashed, and $\mathcal{S}*$ denotes the respective phase shifted pattern, i.e., $\mathcal{S}$`hh` are the phase shifted hot hexagons. `hb` and `cb` both form part of a loop `hs` $\overset{\texttt{hb}}{\to}$ `hh` $\overset{\texttt{r1}}{\to}$ $\mathcal{S}$`ch` $\overset{\mathcal{S}\texttt{cb}}{\to}$ `cs` $\overset{\texttt{cb}}{\to}$ `ch` $\overset{\texttt{r2}}{\to}$ $\mathcal{S}$`hh` $\overset{\mathcal{S}\texttt{hb}}{\to}$ `hs`, where `r1` and `r2` are called rectangles. (b)–(d) `r1` example solutions for which, in the expansion (6), $B > 0$ and A changing from $A>0$ in (b) via $A=0$ in (c) to $A<0$ in (d). (e)–(f) `r2` with $B < 0$ and A changing from $A<0$ in (e) via $A=0$ in (f) to $A>0$ in (g). All domains as in Fig. 1.

domains, these bifurcation points collapse to λ_c, e.g., over the 6×2 domain used in Fig. 4 below we have $\lambda_{10} \approx 3.2042$. Similarly, on all branches shown in Fig. 1 there are very many bifurcation points, and thus we only plot a small part of the full BD. See [UWR12] on details how `pde2path` tries to avoid undesired branch–switching. The `pde2path` script to generate Fig. 1 is also included in the software as demo `schnakenberg`. ⌋

2.2 Fronts, localized patterns, pinning and snaking

Counting from the `hs` branch, `pde2path` yields four bifurcation points `hbbp1`, `hbbp2`, `hbbp3` and `hbbp4` on the hot bean branch. One bifurcating branch connects `hbbp1` and `hbbp4`, and another branch connects `hbbp2` and `hbbp3`.

By doubling the horizontal length to a 4×2 domain, i.e., setting $l_x = 8\pi/k_c$, we find eight bifurcation points `hbbp1`,...,`hbbp8` on `hb`, see Fig. 3. The branches bifurcating in `hbbp1` and `hbbp2` are called `hf` (hot front) and `hl` (hot localized), respectively. Some example solutions on `hf` and `hl` are also presented, and the so called Ginzburg–Landau Maxell point λ_m. The `hf` branch connects `hbbp1` to `hbbp8`, and contains stationary fronts U_{het} from hot spots to hot stripes, while `hl` connects `hbbp2` to `hbbp7` and contains homoclinic solutions U_{hom} in the form of localized hot stripes embedded in hot spots. Both branches show a snaking behaviour in the BD, and we first discuss the `hl` branch in (a) which indicates the start of so called homoclinic snaking, which becomes more prominent if we further increase the domain size.

The idea is that on `hl`, looking from `hbbp7` to `hbbp2`, during each cycle consisting of two folds, a further roll is added on both sides of the roll pattern localized in the middle over a background of hexagons. After every second saddle-node the branch contains stable solutions. In contrast to theory and also to 1D problems over really large domains, the branch does not snake around a vertical line but in a slanted manner. This, and the fact that the branch does not directly bifurcate from the stripes but from the beans, are finite size effects, cf. [BCR08, BBKM08, HK09, Daw09]. During, e.g., the initial traverse from `hbbp7` to `hl172` the "near hexagon bean pattern" at the bifurcation point is reshaped to spots at the sides and stripes in the middle. The analogous reshaping to "near stripe beans" takes place between `hl96` and `hbbp2`. By symmetry there is also a branch of localized hot spots embedded in hot stripe patterns (not shown).

Remark 2.4. For, e.g., the 1D cubic quintic SHe (2), an analogon of the bean branch is the branch r_- of small amplitude unstable rolls that bifurcates subcritically from $(u, \lambda) = (0, 0)$ and "connects" to the fold where the rolls become stable. In [Daw09] the appearance of bifurcation points on r_- is related to modulational instability of the amplitudes $A_-(\lambda)$ of the unstable rolls in the associated Ginzburg–Landau equation, derived by using a scaling of the "subcriticallity parameter" ν in (2). In particular, this gives a lower bound on the domain size necessary for these bifurcations, which is linear in $1/\nu$, i.e., inversely proportional to the subcriticality parameter. Moreover, it explains why the bifurcations occur in connected pairs like (in our case) `hbbp1` – `hbbp8`, `hbbp2` – `hbbp7`, and so on.

At least the relation between subcriticality of the equation and necessary domain size for secondary bifurcations also holds for our system, see Remark 2.5. We expect that calculations similar to those in [Daw09] can also be done in our case using the system of Ginzburg–Landau equations derived in §3, but naturally they will be more complicated. ⌋

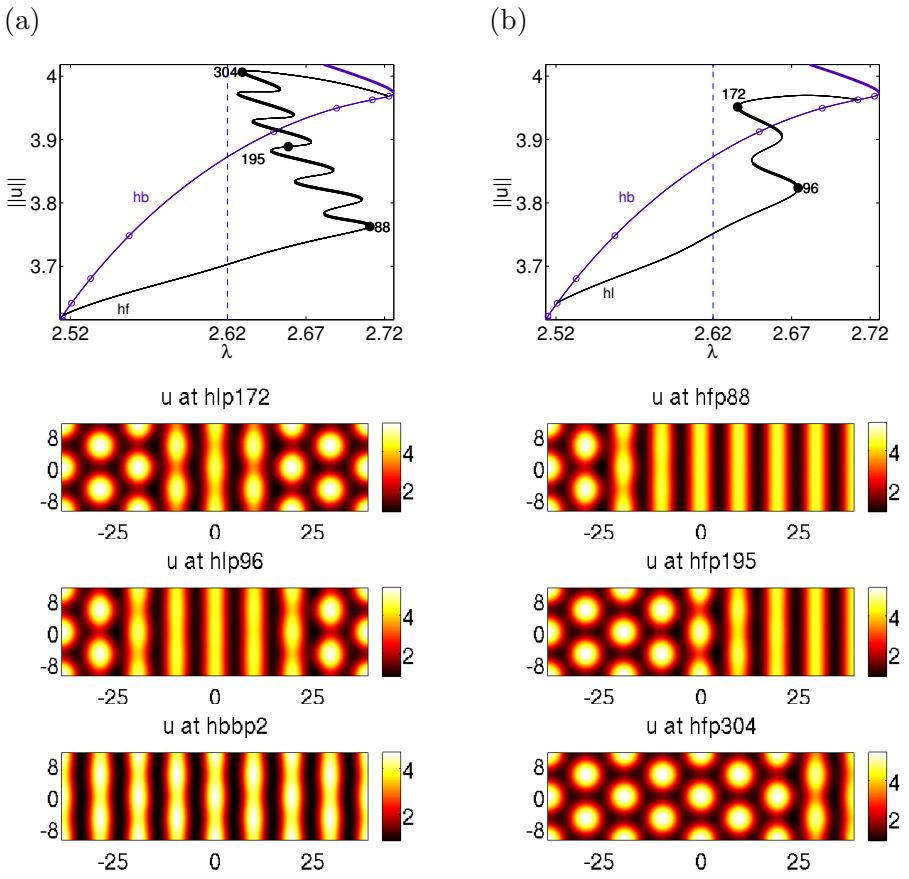

Figure 3: Bifurcation diagrams and example plots of fronts and localized patterns of (4) obtained with `pde2path` over a 4×2 domain. Here $\|u\| = \|u\|_{L^8} := \left(\frac{1}{|\Omega|}\int_\Omega |u(x,y)|^8 \mathrm{d}(x,y)\right)^{1/8}$, which was chosen purely for graphical reasons, and $\lambda_m \approx 2.62$ is the so called (Ginzburg–Landau) Maxwell point, see §3. (a) shows the branch of localized patterns `hl` connecting the second and the seventh bifurcation points of the hot bean branch. Bifurcation points are indicated by $\circ$, stable and unstable parts of branches by thick and thin lines, respectively. `hbbp2` stands for the first bifurcation point on `hb`. (b) shows the branch `hf` of hot fronts connecting `hbbp1` and `hbbp8`.

In contrast to the homoclinic snaking in (a) which at least for simpler models on infinite cylinders

can be also explained and predicted theoretically, see §3, finite size and numerical effects should be regarded as essential for the "heteroclinic snaking" in (b). In fact, at least for the 1D Swift–Hohenberg equation, beyond all order asymptotics [CK09] predict that for each λ near the Maxwell point there are at most two pinned front solutions, again see §3. Thus we believe that the fronts in (b) should be seen as homoclinics by even extension of the solutions over the left boundary (spots on a background of rolls) or right boundary (stripes on a background of spots).

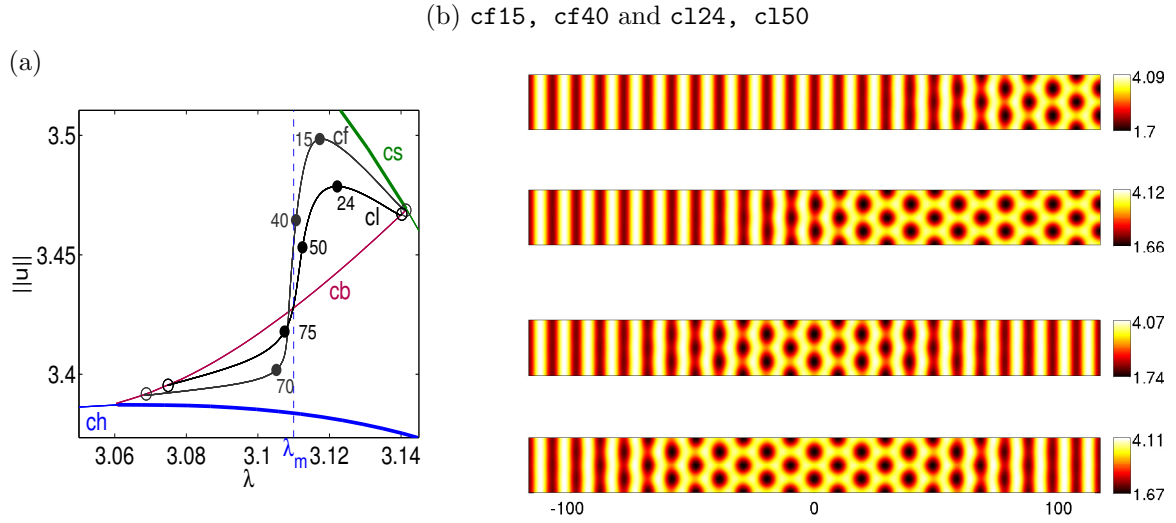

Figure 4: Bifurcation from the cold beans on a 12×2 domain. (a) `cf` branch connecting `cbbp1` with `cbbp8` in a monotonous way (no snaking), cold localized branch `cl`, and the cold Maxwell point (see §3). (b) some example solutions.

On the cold bean branch `cb` there are no bifurcation points over a 2×2 or 4×2 domain (see Remark 2.5 below for further discussion). However, Fig.4(a) shows 4 of the 8 bifurcation points obtained on the cold bean branch over a 12×2 domain, namely `cbbp1, cbbp2, cbbp7, cbbp8`, the branch `cf` (cold front) connecting `cbbp1` and `cbbp8`, and the branch `cl` connecting `cbbp2` and `cbbp7`, and consisting of spots on a stripe background. Panel (b) shows 4 example solutions. In, e.g., `cl50` it can be seen that the localized spots are shifted by $2\pi/k_c$ in x, such that here we really consider $\mathcal{S}$`cb` which connects `cs` to $\mathcal{S}$`ch`, cf. Remark 2.1, but for simplicity we omit the $\mathcal{S}$.

Similar to Fig. 3, after bifurcation from, e.g., `cbbp1`, in the traverse to `cf15` the solutions reshape into stripes on the left and spots on the right. The growth of the hexagon part then happens in a narrow λ regime around λ_m between `cf15` and `cf70`, while between `cf70` and `cbbp8` the solutions are reshaped to spot-like beans. Similar remarks hold for the `cl` branch.

Remark 2.5. An essential difference to Fig. 3 is that there is no snaking behaviour of the `cf` and `cl` branches. Following Remark 2.4 we believe that the need for a large domain to obtain bifurcations from the `cb` branch can be explained from the "weak subcriticality" of the system in this range. This means that the cold bistable range is rather narrow, compared to the hot bistable range. In other words, the difference in (Ginzburg–Landau–)energy between the `ch` amplitudes and the `cs` amplitudes is much smaller than between the `hh` and `hs` solutions in their bistable range, and this results in flatter fronts for the associated Ginzburg–Landau system.

However, here increasing the domain gives bifurcation points on `cb` (e.g., 4 on a 6×2 domain), and branches connecting the first and the last, the second and the second to last, and so on, as in [Daw09], but no snaking. Presently we do not know if this non–snaking is still due to numerical and finite size effect, but rather conjecture that it is not: Increasing the domain size, the steep part near λ_m becomes steeper, but our numerics suggest that this process converges to a monotonous

in λ branch. *If* there is snaking in these branches over finite domains, then it is in a very narrow λ interval, and one needs *very* large domains and fine discretizations.

Similar effects are also observed in [HO05] for the 1D cubic quintic SHe (2) without a scaling assumption on ν. For $0 < \nu = \mathcal{O}(1)$ there are branches which connect points on r_- (unstable small amplitude rolls) near zero with points on r_- near the fold, but only for sufficiently large (fixed) ν they become steep in parameter λ and eventually start to snake in the bifurcation diagram ($\nu > 1.5$, which agrees with the numerics in [DMCK11, Figure 1] for (2) with $\nu = 1.6$ and a rather narrow snake). ⌋

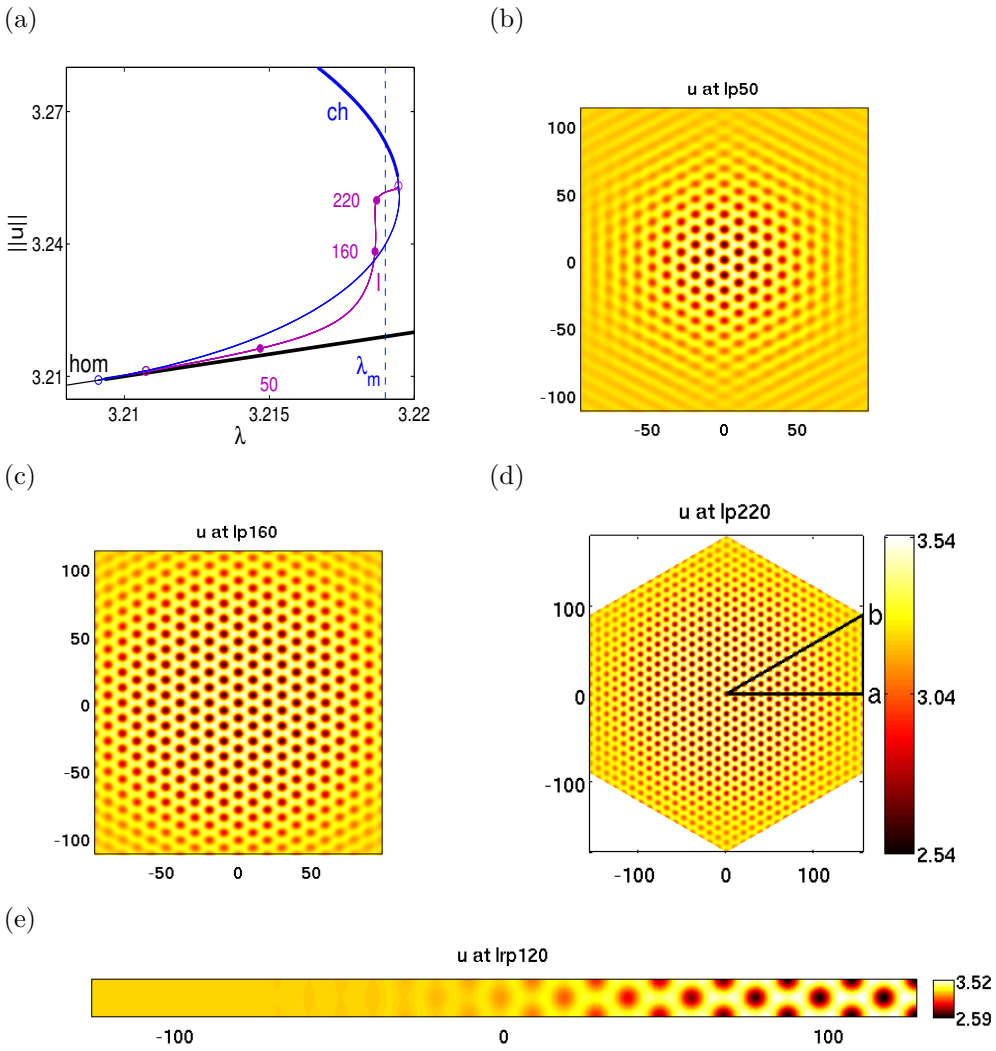

Figure 5: Bistable range between homogeneous solution and cold hexagons. (a) partial BD and the homogeneous Maxwell point (see §3). Additional to quasi 1D solutions we find fully 2D localized hexagon patches. The triangle in (d) indicates the computational domain with $a = (32\pi/k_c, 0)$ and $b = (32\pi/k_c, 32\pi/(\sqrt{3}k_c))$, and about 90.000 triangles. We use Neumann BC on all three sides and for plotting first make an even extension over $y = 0$ and then five rotations by 60 degrees. (e) quasi 1D front between $w = (\lambda, 1/\lambda)$ and spots on a 13×1 domain, $\lambda \approx 3.219$.

The third bistable we discuss is between the homogeneous solution $w^* = (\lambda, 1/\lambda)$ and the cold spots for $3.21 \approx \lambda_c < \lambda < \lambda_{cb} \approx 3.22$. Here, over sufficiently large domains, we have bifurcation points on the small amplitude (unstable) cold spot branch, which now corresponds to the r_-

branches for (2) mentioned in Remarks 2.4 and 2.5, and as above we can find quasi 1D fronts between w^* and cold spots, see Fig. 7(e), and the associated 1D localized patterns. However, as in the qcSHe (1) and the cqSHe (2), see [ALB$^+$10] and the references therein, we can also calculate fully localized patches of hexagons, see Fig. 7(a)–(d). In contrast to [ALB$^+$10], none of these branches shows snaking (in our numerics, over any of the domains we considered), and again we conjecture that this is due to the very weak subcriticality, or, in other words, the very weak difference in Ginzburg–Landau energy between w^* and the cold spots.

3 Ginzburg-Landau reduction

We now approximate the spots, stripes and mixed modes by the Landau formalism, and the various fronts and localized patterns by the Ginzburg–Landau formalism. In particular, using an energy argument and the so called Maxwell point for the Ginzburg–Landau system we find an approximate prediction where to find the hot snaking and the cold fronts in the bifurcation diagram for (4). Similar ideas are worked out much more deeply for the 1D quadratic–cubic SHe (1) in [CK09] and the cubic–quintic SHe (2) in [DMCK11], where, by augmenting the Ginzburg–Landau ansatz with beyond all order asymptotics, accurate bifurcation diagrams for homoclinic snaking were rigorously derived.

In our case we need a system of Ginzburg–Landau equations, and our analysis is more formal since even a consistent derivation of the Ginburg–Landau system is difficult as we refrain from scaling assumptions for quadratic interactions but rather work with the numerical coefficients in (4). However, from the Ginzburg–Landau system we calculate the Maxwell point as a necessary condition for Ginzburg–Landau fronts, and the pinning argument from [Pom86] then suggest the existence of stationary fronts for (4). This approximation turns out to be qualitatively and at least in the cold regime also quantitatively correct, and thus it gives a lowest order approximation for the numerical solutions, although it cannot explain the snaking.

3.1 Landau description of spots, stripes, and mixed modes

To formally reduce (4) to a Ginzburg-Landau system the idea is to treat x as an unbounded variable, while $y \in [-\frac{m\pi}{\sqrt{3}k_c}, \frac{m\pi}{\sqrt{3}k_c}]$ with Neumann boundary conditions, as in the numerics. At least close to λ_c the most unstable modes are then $e_1\Phi$, $e_2\Phi$, and $e_3\Phi$, where $e_1 = \mathrm{e}^{\mathrm{i}k_c x}$, $e_2 = \mathrm{e}^{\mathrm{i}k_c(-x+\sqrt{3}y)/2}$, $e_3 = \mathrm{e}^{\mathrm{i}k_c(-x-\sqrt{3}y)/2}$, and $\Phi = \Phi(\lambda) \in \mathbb{R}^2$ is the eigenvector of $\hat{L}(k_c, \lambda)$ to the eigenvalue $\mu_+(k_c, \lambda)$. First we consider slowly varying complex amplitudes $A_j = A_j(t)$ of these modes, $j = 1, 2, 3$, i.e., our ansatz reads

$$w = \sum_{i=1}^{3} A_i e_i \Phi + \frac{1}{2}\sum_{i=1}^{3} |A_i|^2 \phi_0 + \sum_{i=1}^{3} A_i^2 e_i^2 \phi_1 + \sum_{1\le i<j\le 3} A_i \overline{A_j} e_i \overline{e_j} \phi_2 + \text{c.c.} + \text{h.o.t.}, \tag{7}$$

where $\overline{A}_j$ means the complex conjugate of A_j and c.c. stand for the complex conjugate of all preceding terms. The vectors ϕ_0, ϕ_1, and ϕ_2 are introduced to remove quadratic terms at wave vectors $\mathbf{k}$ with $k = 0$, $k = 2k_c$ and $k = \sqrt{3}k_c$ from the residual $L(\Delta)w + G(w)$.

The calculations are best organized by writing (5) in the form

$$\partial_t w = L(\Delta)w + B(w, w) + C(w, w, w), \tag{8}$$

where B and C are symmetric bilinear and trilinear forms. To remove terms of order $A_i A_j$ from (4) we need

$$\begin{aligned} &\phi_0(\lambda) = -2\hat{L}(0, \lambda)^{-1} B(\Phi, \overline{\Phi}), \qquad \phi_1(\lambda) = -\hat{L}(2k_c, \lambda)^{-1} B(\Phi, \Phi), \\ &\phi_2(\lambda) = -2\hat{L}(\sqrt{3}k_c, \lambda)^{-1} B(\Phi, \overline{\Phi}). \end{aligned} \tag{9}$$

These terms arise due to quadratic interactions of the forms, e.g., $B(A_1e_1\Phi, \overline{A_1e_1\Phi}) = |A_1|^2B(\Phi,\overline{\Phi})$, $B(A_1e_1\Phi, A_1e_1\Phi) = A_1^2\mathrm{e}^{2\mathrm{i}k_cx}B(\Phi,\Phi)$, and $B(A_1e_1\Phi, \overline{A_2e_2\Phi}) = A_1\overline{A_2}\mathrm{e}^{\mathrm{i}\frac{k_c}{2}(3x-\sqrt{3}y)}B(\Phi,\overline{\Phi})$. Allthough $\Phi\in\mathbb{R}^2$ in our case we keep the notation $\overline{\Phi}$ as this makes it easier to see where the respective terms come from. The matrices $\hat{L}(0,\lambda)$, $\hat{L}(2k_c,\lambda)$ and $\hat{L}(\sqrt{3}k_c,\lambda)$ are invertible at least for λ not too far from λ_c. From the Fredholm alternative we obtain the Landau ODE system as the solvability conditions for removing terms up to cubic order, namely

$$\begin{aligned}
\text{at } e_1: &\quad \partial_t A_1 = f_1(A_1,A_2,A_3) := c_1A_1 + c_2\overline{A_2A_3} + c_3|A_1|^2A_1 + c_4A_1(|A_2|^2+|A_3|^2),\\
\text{at } e_2: &\quad \partial_t A_2 = f_2(A_1,A_2,A_3) := c_1A_2 + c_2\overline{A_1A_3} + c_3|A_2|^2A_2 + c_4A_2(|A_1|^2+|A_3|^2),\\
\text{at } e_3: &\quad \partial_t A_3 = f_3(A_1,A_2,A_3) := c_1A_3 + c_2\overline{A_1A_2} + c_3|A_3|^2A_3 + c_4A_3(|A_1|^2+|A_2|^2),
\end{aligned} \tag{10}$$

with $c_1(\lambda) = \mu_+(k_c,0,\lambda)$, $c_2(\lambda) = 2\langle B(\overline{\Phi},\overline{\Phi}),\Phi^*\rangle$, $c_3(\lambda) = \langle 3C(\Phi,\Phi,\overline{\Phi}) + 2B(\overline{\Phi},\phi_1) + 2B(\Phi,\phi_0),\Phi^*\rangle$, and $c_4(\lambda) = \langle 6C(\Phi,\Phi,\overline{\Phi}) + 2B(\Phi,\phi_2) + 2B(\Phi,\phi_0),\Phi^*\rangle$. Here $\Phi^*(\lambda)$ is the adjoint eigenvector of $\hat{L}(k_c,\lambda)$ to the eigenvalue $\mu_+(k_c,\lambda)$, normalized such that $\langle\Phi,\Phi^*\rangle = 1$. At $\overline{e_j}$, $j=1,2,3$, we obtain the complex conjugate equations. See, e.g., [GSK84, Pom86], [CH93, §IV,A,1,a(iii)], [DSSS03, §2], [Hoy06, §5],[NG06, Pis06], which also explain that (10) is the generic form of the amplitude equations for hexagonal symmetry. The crucial step is the actual calculation of the coefficients.

Remark 3.1. In (7), $\Phi = \Phi(k_c,\lambda)$ varies with λ and is not fixed at $\lambda=\lambda_c$, which would be the more classical ansatz. Similarly, terms like (9) and the coefficients $c_2,\dots,c_4$ are evaluated at λ, not as usual at $\lambda=\lambda_c$. The formalisms are in fact equivalent for $\lambda\to\lambda_c$ with the differences hidden in the h.o.t. in (7). The reason why we always evaluate at λ is that we want to use the formalism also for $\lambda_c-\lambda=\mathcal{O}(1)$ and then expect (and find) better approximations with $\Phi=\Phi(\lambda)$. On the other hand, for the comparison with the numerics we want to keep the wave vectors fixed and thus evaluate at k_c, which approximately stays the most unstable wave number also for $\lambda_c-\lambda{=}\mathcal{O}(1)$. ⌋

From the coefficients $c_j(\lambda)$, $j=1,\dots,4$, see Fig. 6(a), it follows that

$$T_\pm = \pm\sqrt{-\frac{c_1}{c_3}} \quad\text{and}\quad P_\pm = -\frac{c_2}{2(c_3+2c_4)} \pm \sqrt{\frac{c_2^2}{4(c_3+2c_4)^2} - \frac{c_1}{c_3+2c_4}}, \tag{11}$$

are real in the Turing-unstable range $\lambda<\lambda_c$, respectively for $\lambda<\lambda_{\mathrm{GLfold}}\approx\lambda_{cb}\approx 3.22$. The triples $(T_+,0,0)$, $(T_-,0,0)$, (P_+,P_+,P_+), and (P_-,P_-,P_-) solve (10) and via (7) generate hot stripes, cold stripes, hot spots, and cold spots, respectively. Mixed modes are obtained from setting $A_3=A_2$ and solving (10) for (A_1,A_2). The formulas, together with the signs of $c_j(\lambda)$, also explain the supercritical pitchfork bifurcation of stripes, and the transcritical bifurcation of the spots. Figures 6(b),(c) show the complete BD for stationary solutions of (10) in the invariant subspace $A_1=:A\in\mathbb{R}$ and $A_2=A_3=:B\in\mathbb{R}$, while (d),(e) compares the BD of stripes, spots and beans for (10) with the numerical BD from Fig. 1 for the full system (4). Though qualitatively correct down to $\lambda=2.4$, the approximation errors grow with $|\lambda-\lambda_c|$, as expected. Additionally to the L^∞ like error already shown, for $i\in\{\text{stripes,spots}\}$ we define the relative L^1 errors

$$z_i = \sum_{(x,y)\in\Omega_d} \|U_{\mathrm{num},i}(x,y) - U_i(x,y)\|_1 \Big/ \sum_{(x,y)\in\Omega_d} \|U_{\mathrm{num},i}(x,y)\|_1 \tag{12}$$

between the numerical solutions U_{num} and approximate solutions $U=w^*+w$ from (7), where Ω_d is the discretization used to calculate the numerical solution from Fig. 1. It turns out that z_{stripes} stays rather small also for $\lambda_c-\lambda=\mathcal{O}(1)$, while z_{hex} behaves worse, see Fig. 6(f), and also Remark 4.1 for further comments.

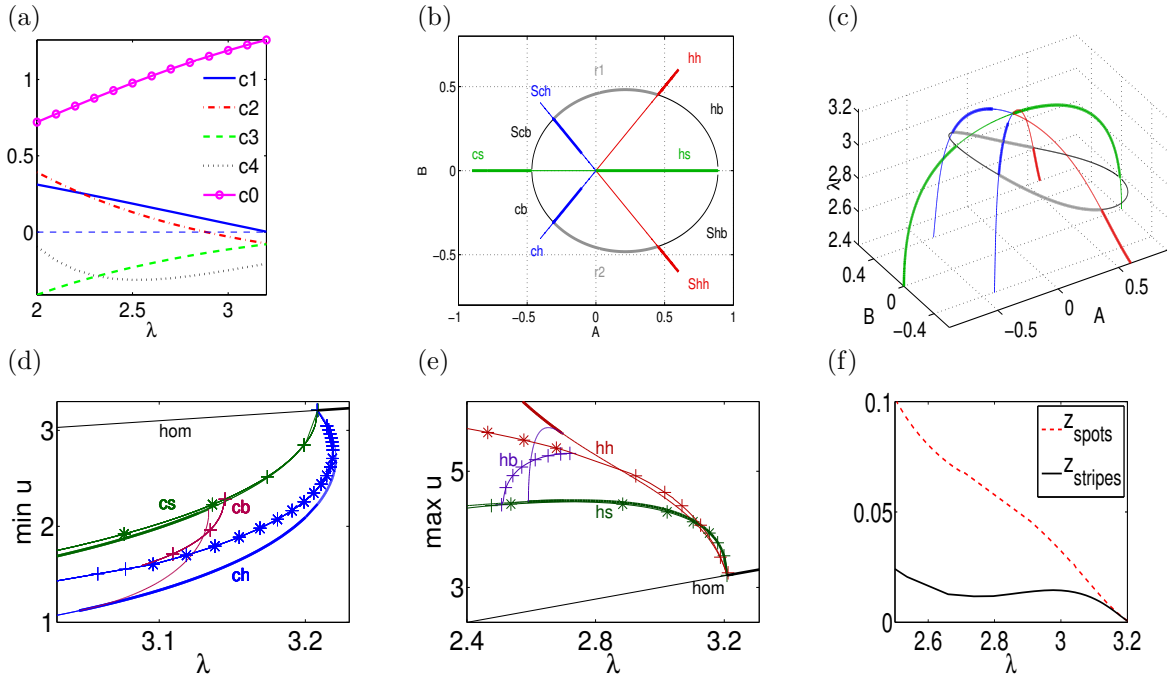

Figure 6: (a) Landau coefficients, and Ginzburg–Landau coefficient c_0, see §3.2. (b),(c) Landau BD in the invariant subspace $A_1 =: A \in \mathbb{R}$ and $A_2 = A_3 =: B \in \mathbb{R}$, stability/instability indicated by thick/thin lines. (d),(e) Comparisons of numerical BD from Fig. 1 (indicated by * for stable points and + for unstable points) with Landau BD near the cold and hot bistable regimes. (f) relative L^1 errors between hot numerical and Landau solutions defined in (12).

Another notable discrepancy between the Landau BD and the (numerical) BD for (4) is that in the former the (hot) stripes are stable all the way to the bifurcation point, while in the PDE this depends on the domain size. On a 1×1 domain we obtain exactly the same stability as displayed in Fig. 6(b),(c), and the instability near bifurcation of the stripes already on a 2×2 domain as in Fig. 1 is due to a long zig-zag instability, which is not captured in our Landau ansatz. Similar remarks apply for instance to the rectangle branches, which are mostly unstable for (4) over a 2×2 domain.

3.2 Ginzburg–Landau formalism and fronts

Motivated by the acceptable approximation of the spots, stripes and beans via (7) and (10) we proceed to use the Ginzburg–Landau (GL) reduction to predict the stationary fronts and localized patterns. If instead of $A_j = A_j(t)$ we assume that $A_j = A_j(t, x)$ are slowly varying functions also of $x \in \mathbb{R}$, then instead of the Landau system (10) we obtain the Ginzburg–Landau system

$$\partial_t A_1 = c_0 \partial_x^2 A_1 + f_1(A_1, A_2, A_3), \quad \partial_t A_j = \frac{c_0}{4} \partial_x^2 A_j + f_j(A_1, A_2, A_3), \ j = 2, 3, \tag{13}$$

where $c_0(\lambda) = -\frac{1}{2}\partial_{k_1}^2 \mu_+((k_c, 0), \lambda) > 0$. See [Sch94, BvHS95, Sch99, Mie02] for background on this formal procedure, and for so called attractivity and approximation theorems which estimate the difference between a true solution of (3) and an approximation described by (7) and (13), close to bifurcation. Thus, these theorems involve some small amplitude assumption for (u, v), related slow scales for t and x in $A_j(t, x)$, and, for the present case of three resonant modes, a suitable scaling for the quadratic interactions, i.e., small c_2.

Here we again want to use the GL system (13) at an $\mathcal{O}(1)$ distance from λ_c and find a necessary condition for stationary fronts between spots like $A \equiv (P_+, P_+, P_+)$ and stripes like $A \equiv (T_+, 0, 0)$ in (13). Thus we consider the stationary Ginzburg–Landau system

$$c_0\partial_x^2 A_1 + f_1(A_1, A_2, A_3) = 0, \quad \frac{c_0}{4}\partial_x^2 A_j + f_j(A_1, A_2, A_3) = 0, \ j = 2, 3, \tag{14}$$

as a dynamical system in the spatial variable x. Now restricting to real amplitudes A_j, the total energy of (14) is given by $E_{\text{total}} = E_{\text{kin}} + E_{\text{pot}}$, where

$$E_{\text{kin}} = \frac{c_0}{2}\left((\partial_x A_1)^2 + \frac{1}{4}(\partial_x A_2)^2 + \frac{1}{4}(\partial_x A_3)^2\right), \quad \text{and}$$
$$E_{\text{pot}} = \sum_{i=1}^{3}\left(\frac{c_1}{2}A_i^2 + \frac{c_3}{4}A_i^4\right) + c_2 A_1 A_2 A_3 + \frac{c_4}{2}(A_1^2A_2^2 + A_1^2A_3^2 + A_2^2A_3^2)$$

are the kinetic and potential energy, respectively. Then $\frac{d}{dx}E_{\text{total}} = 0$, i.e., E_{total} is conserved. Thus, a necessary condition for, e.g., a heteroclinic orbit A_{front} between (P_+, P_+, P_+) and $(T_+, 0, 0)$ to exist in (14) is $E_{\text{pot}}(T_+, 0, 0) = E_{\text{pot}}(P_+, P_+, P_+)$. Again we first focus on the hot bistable range and in Fig. 7(a) plot $E_{\text{pot}}(T_+, 0, 0)$ and $E_{\text{pot}}(P_+, P_+, P_+)$. Their intersection defines the so called (hot) Maxwell point λ_m. Though we refrain from discussing the general energy landscape and dynamics of (14), it turns out that at least numerically the necessary condition $\lambda = \lambda_m$ is also sufficient. Figure 7(b) shows a stationary front for (13) (with Neumann boundary conditions), which can either be obtained from time evolution of (13) with a suitable initial guess, or from solving the stationary boundary value problem. See also [MNT90] for some more analysis for front solutions of (14), including some implicit solution formulas. On the other hand, for $\lambda < \lambda_m$ with $E_{\text{pot}}(T_+, 0, 0) < E_{\text{total}}(P_+, P_+, P_+)$ we obtain a front for (13) *travelling* towards higher energy, i.e., (P_+, P_+, P_+) invades $(T_+, 0, 0)$, and vice versa for $\lambda > \lambda_m$.

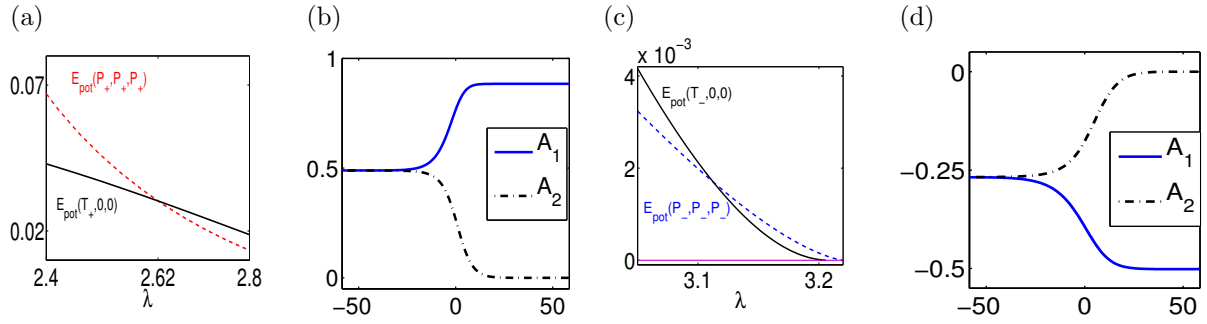

Figure 7: (a), (c) Energies of spots and stripes near the hot resp. cold bistable regimes; their intersections define the respective Maxwell points $\lambda = 2.62$, $\lambda = 3.11$, and the zero of $E_{\text{pot}}(P_-, P_-, P_-)$ defines the third Maxwell point $\lambda = 3.219$. Hot (b) and cold (d) stationary Ginzburg–Landau fronts between stripes and spots at the respective Maxwell points, for comparison both over domain $[-12\pi/k_c, 12\pi/k_c]$, $A_3 = A_2$.

Thus, from the GL approximation *standing* fronts U_{het} between different patterns are only predicted at precisely $\lambda = \lambda_m$. In the physics literature, e.g., [Pom86], the basic argument for the existence of U_{het} in an interval around λ_m is that the patterns create an effective periodic potential which yields a pinning of fronts.

It is not obvious whether the stationary GL system (14) has homoclinic solutions A_{hom} with, say, $A_{\text{hom}}(x) \to (P_+, P_+, P_+)$ as $x \to \pm\infty$, and that pass near $(T_+, 0, 0)$ near $x = 0$. However, (suitably shifted) fronts $A_{\text{front}}(x_0 + \cdot)$ and "backs" $A_{\text{back}}(x_1 + \cdot)$ with $A_{\text{back}}(x) = A_{\text{front}}(-x)$ can be glued together to give approximate homoclinics with long plateaus but also with some dynamics in

time which can be expected to be exponentially slow in the separation distance between A_{front} and A_{back}, [CP90]. In fact we can generate almost stationary pulses numerically, but eventually the solution decays to a homogeneous rest state $(T_+, 0, 0)$ or (P_+, P_+, P_+). Similarly, (14) may have periodic orbits which stay close to (P_+, P_+, P_+) resp. $(T_+, 0, 0)$ over very long x-intervals. Clearly, for these "approximate homoclinics" a similar pinning argument as for the heteroclinics can be applied and predicts the existence of localized patterns as in Fig. 3(b) near the Maxwell point λ_m.

In [CK09, DMCK11] it is worked out mathematically that the pinning and hence also the snaking are exponentially small effects and thus cannot be predicted at any order by Ginzburg–Landau type asymptotic expansions alone. However, combining a (high order) Ginzburg–Landau ansatz with beyond all order asymptotics, snaking in the model problems (1) and (2) can be described very accurately. See also, e.g., [Kno08, ALB$^+$10] and the references therein for alternative arguments explaining the snaking via so called heteroclinic tangles in the spatial dynamics formulation of again (1) and (2).

The same pinning arguments apply to the cold bistable range, but the difference to the hot range is that cold Ginzburg–Landau fronts are flatter and wider since relatively to the vector fields f_1, f_2 the diffusion constant c_0 is much larger in the cold range than in the hot range. See Fig. 7(d). As a consequence, snaking might not exist between cold stripes and spots, or if it does exist, then it might be very difficult to find numerically over bounded domains, cf. Remark 2.5, and similarly for fronts between the homogeneous solution and the cold hexagons.

4 Discussion

As for fronts between patterns and homogeneous solutions, the main ingredients for fronts U_{het} between two different periodic patterns is a bistable range, usually generated by a subcritical bifurcation (of mixed modes, in the case of two patterns), and the existence of a heteroclinic connection A_{het} between the corresponding fixed points in the associated Ginzburg–Landau system at some Maxwell point $\lambda = \lambda_m$. The pinning effect in the full system then yields the existence of U_{het} in a parameter interval around λ_m, and the same effect yields branches of localized patterns U_{hom} in a patterned background even if the Ginzburg–Landau system only has "approximate" homoclinic solutions.

These findings have already been suggested in [Pom86], and been further worked out in 1D problems and for patterns over homogeneous background in various papers, e.g., [BK07, Kno08, CK09, ALB$^+$10, DMCK11], but the present paper appears to be the first numerical illustration for different patterns in 2D. Moreover, our numerics suggest that over bounded domains these branches may only snake if the bistability is sufficiently strong. These numerics are somewhat delicate due to the very many solution branches that exist in the Turing unstable range, in particular over large domains, which requires rather fine discretizations to avoid uncontrolled branch switching.

Here we restricted to domains of still intermediate size, and this might be the reason why we were not able to generate snaking branches of fronts and localized patterns near the cold beans (Fig. 4) or near λ_c (Fig. 7). For us it is an open roblem whether these branches start to snake over much larger domains. Close to the primary bifurcation we have a good Ginzburg–Landau approximation and possibly a beyond all orders expansion could be started [CK09, DMCK11], but the snaking region might be very narrow and thus resolution of the snaking might require very large domains and very accurate numerics.

The results are certainly not special for the model problem (4); we have used the same method to predict and numerically find various pinning branches in other 2D reaction diffusion systems [WF13] which are slightly more complicated algebraically due to Holling type nonlinearities, but for the same reason in fact nicer for the numerics. Interestingly, there all the pinning branches show snaking.

Remark 4.1. An ad hoc way to derive a Landau system like (10) from a system like (4) is to *only* consider the solvability conditions (10) at the critical modes without first removing the A^2 residual at second harmonics. This amounts to the ansatz $w = \sum_{i=1}^{3} A_i e_i \Phi + \text{c.c.}$, or in other words setting $\phi_0, \phi_1, \phi_2 = 0$ in (9). As this yields a residual of order A^2 we call this the A^2 ansatz and denote the new coefficients in (10) by c_{32} and c_{42}. This is obviously simpler than (7), but not formally consistent. However, at order $\mathcal{O}(1)$ distance from the bifurcation the A^2 ansatz *may* give a better approximation of solutions than the residual of order A^3 ansatz (7), since (7) represents only an asymptotic expansion, and not the first terms in some convergent series.

It turns out that in some sense this is indeed the case for (4), and this can be used to improve the prediction of the Maxwell point. While in the hot bistable range the A^2 ansatz gives a much larger error for the stripes, its error for the hot spots is in fact smaller than the one in Fig. 6(c). The idea is to use the coefficients $c_3(\lambda)$ from the A^3 ansatz for the stripes and the coefficients $c_{32}(\lambda)$ from the A^2 ansatz for the spots ($|c_4(\lambda) - c_{42}(\lambda)|$ is very small anyway) in a "mixed" Ginzburg–Landau system that retains the variational structure. Thus, let S be T_+ and H be P_+ determined by using the A^3- and A^2-ansatz, respectively, and consider the system

$$\begin{aligned}
&c_0\partial_x^2 A_1 + c_1 A_1 + c_2 A_2 A_3 + \left(c_{33}\left(\frac{A_1 - H}{S - H}\right) + c_{32}\left(\frac{A_1 - S}{H - S}\right)\right) A_1^3 + c_4 A_1(A_2^2 + A_3^2) = 0,\\
&\frac{c_0}{4}\partial_x^2 A_2 + c_1 A_2 + c_2 A_1 A_3 + \left(c_{33}\left(\frac{A_2 - H}{S - H}\right) + c_{32}\left(\frac{A_2 - S}{H - S}\right)\right) A_2^3 + c_4 A_2(A_1^2 + A_3^2) = 0, \qquad (15)\\
&\frac{c_0}{4}\partial_x^2 A_3 + c_1 A_3 + c_2 A_1 A_2 + \left(c_{33}\left(\frac{A_3 - H}{S - H}\right) + c_{32}\left(\frac{A_3 - S}{H - S}\right)\right) A_3^3 + c_4 A_3(A_1^2 + A_2^2) = 0.
\end{aligned}$$

In the hot bistable range we have $S > H$ such that (14) is well-defined in this range. Moreover, (15) has again a conserved energy $E_{\text{total}} = E_{\text{kin}} + E_{\text{pot}}$ where now

$$E_{\text{pot}} = \sum_{i=1}^{3} \frac{c_1}{2} A_i^2 + c_2 A_1 A_2 A_3 + c_{33} A_i^4 \frac{\frac{1}{5}A_i - \frac{1}{4}H}{S - H} + c_{32} \sum_{i=1}^{3} A_i^4 \frac{\frac{1}{5}A_i - \frac{1}{4}S}{H - S} + \frac{c_4}{2}(A_1^2 A_2^2 + A_1^2 A_3^2 + A_2^2 A_3^2).$$

Using this energy to calculate the Maxwell–point for (15) we find $\lambda_m = 2.67$ which is more in the center of the snaking region than $\lambda_m = 2.62$. Thus, using the additional information that the spots are better approximated by the A^2 ansatz than by the A^3 ansatz we can obtain a better prediction for the Maxwell point. ⌋

References

[ALB+10] D. Avitabile, D.J.B. Lloyd, J. Burke, E. Knobloch, and B. Sandstede. To snake or not to snake in the planar Swift-Hohenberg equation. *SIAM J. Appl. Dyn. Syst.*, 9(3):704–733, 2010.

[BBKM08] A. Bergeom, J. Burke, E. Knobloch, and I. Mercader. Eckhaus instability and homoclinic snaking. *Phys.Rev.E*, 78:025201, 2008.

[BCR08] U. Bortolozzo, M. G. Clerc, and S. Residori. Local theory of the slanted homoclinic snaking bifurcation diagram. *Phys. Rev. E*, 78:036214, Sep 2008.

[BK06] J. Burke and E. Knobloch. Localized states in the generalized Swift-Hohenberg equation. *Phys. Rev. E*, 73:056211, May 2006.

[BK07] J. Burke and E. Knobloch. Homoclinic snaking: Structure and stability. *Chaos*, 17(3):037102, 15 p., 2007.

[BKL+09] M. Beck, J. Knobloch, D.J.B. Lloyd, B. Sandstede, and T. Wagenknecht. Snakes, ladders, and isolas of localized patterns. *SIAM J. Math. Anal.*, 41(3):936–972, 2009.

[BvHS95] P. Bollermann, A. van Harten, and G. Schneider. On the justification of the Ginzburg–Landau approximation. In A. Doelman and A. van Harten, editors, *Nonlinear dynamics and pattern formation in the natural environment*, pages 20–37. Longman UK, 1995.

[CH93] M.C. Cross and P.C. Hohenberg. Pattern formation outside equilibrium. *Rev. Mod. Phys.*, 65:854–1190, 1993.

[CK09] S.J. Chapman and G. Kozyreff. Exponential asymptotics of localised patterns and snaking bifurcation diagrams. *Physica D*, 238(3):319–354, 2009.

[CP90] J. Carr and R. Pego. Invariant manifolds for metastable patterns in $u_t = \varepsilon^2 u_{xx} - f(u)$. *Proc. R. Soc. Edinb., Sect. A*, 116(1-2):133–160, 1990.

[Daw09] J.H.P. Dawes. Modulated and localized states in a finite domain. *SIAM J. Appl. Dyn. Syst.*, 8(3):909–930, 2009.

[DMCK11] A.D. Dean, P.C. Matthews, S.M. Cox, and J.R. King. Exponential asymptotics of homoclinic snaking. *Nonlinearity*, 24(12):3323–3351, 2011.

[DSSS03] A. Doelman, B. Sandstede, A. Scheel, and G. Schneider. Propagation of hexagonal patterns near onset. *European J. Appl. Math.*, 14(1):85–110, 2003.

[GSK84] M. Golubitsky, J.W. Swift, and E. Knobloch. Symmetries and Pattern selection in Rayleigh-Benard convection . *Physica*, 10 D:249–276, 1984.

[HK09] S. M. Houghton and E. Knobloch. Homoclinic snaking in bounded domains. *Phys.Rev.E*, 80:026210, 2009.

[HMBD95] M. F. Hilali, S. Métens, P. Borckmans, and G. Dewel. Pattern selection in the generalized Swift-Hohenberg model. *Phys. Rev. E*, 51:2046–2052, Mar 1995.

[HO05] Y. Hiraoka and T. Ogawa. Rigorous numerics for localized patterns to the quintic Swift-Hohenberg equation. *Japan J. Ind. Appl. Math.*, 22(1):57–75, 2005.

[Hoy06] R.B. Hoyle. *Pattern formation.* Cambridge University Press., Cambridge, UK, 2006.

[Kno08] E. Knobloch. Spatially localized structures in dissipative systems: open problem. *Nonlinearity*, 21:T45–T60, 2008.

[LJBK11] D. Lo Jacono, A. Bergeon, and E. Knobloch. Magnetohydrodynamic convectons. *J. Fluid Mech.*, 687:595–605, 2011.

[LSAC08] D.J.B. Lloyd, B. Sandstede, D. Avitabile, and A.R. Champneys. Localized hexagon patterns of the planar Swift-Hohenberg equation. *SIAM J. Appl. Dyn. Syst.*, 7(3):1049–1100, 2008.

[Mie02] A. Mielke. The Ginzburg-Landau equation in its role as a modulation equation. In *Handbook of dynamical systems, Vol. 2*, pages 759–834. North-Holland, 2002.

[MNT90] B.A. Malomed, A.A. Nepomnyashchy, and M.I. Tribelsky. Domain boundaries in convection patterns. *Phys.Rev.A*, 42(12):7244–7263, 1990.

[Mur89] J.D. Murray. *Mathematical biology.* Springer-Verlag, Berlin, 1989.

[NG06] A.A. Nepomnyashchy and A.A. Golovin. General aspects of pattern formation. In A.A. Nepomnyashchy and A.A. Golovin, editors, *Self-Assembly, Pattern Formation and Growth Phenomena in Nano-Systems*, pages 1–54. Springer, 2006.

[Pis06] L.M. Pismen. *Patterns and interfaces in dissipative dynamics.* Springer, 2006.

[Pom86] Y. Pomeau. Front motion, metastability and subcritical bifurcations in hydrodynamics. *Physica D*, 23:3–11, 1986.

[Sch79] J. Schnakenberg. Simple chemical reaction systems with limit cycle behaviour. *Journal of Theoretical Biology*, 81:389–400, 1979.

[Sch94] G. Schneider. Error estimates for the Ginzburg–Landau approximation. *ZAMP*, 45:433–457, 1994.

[Sch99] G. Schneider. Global existence results in pattern forming systems – Applications to 3D Navier–Stokes problems –. *J. Math. Pures Appl., IX*, 78:265–312, 1999.

[Sel68] E.E. Sel'kov. Self-oscillations in glycolysis. *European Journal of Biochemistry*, 4(1):79–86, 1968.

[UWR12] H. Uecker, D. Wetzel, and J. Rademacher. pde2path – a Matlab package for continuation and bifurcation in 2D elliptic systems. Preprint, 40p, software available at `www.pde2path.uni-oldenburg.de`, 2012.

[WF13] D. Wetzel and U. Feudel. Snaking between Turing patterns in some benthic predator prey models. In Preparation, 2013.

[Yan04] L Yang. Stable squares and other oscillatory Turing patterns in a reaction-diffusion model. *PRL*, 92(19):198303–1, 2004.